Evaluation of Performance Tradeoffs When Using Mechanically Swept 1-D Linear Arrays for 3-D DCE-US

Elahe Moghimirad, Zhiting Xu, Hong Ding, Jeffrey Bamber, and Emma Harris

***Abstract*—Dynamic contrast-enhanced ultrasound imaging (DCE-US) may be used to characterize tumor vascular perfusion using metrics derived from time–amplitude curves (TACs). The 3-D DCE-US enables generation of 3-D parametric maps of TAC metrics that may inform on how perfusion varies across the entire tumor. The aim of this work was to understand the effect of low temporal sampling (i.e., <1 Hz) typical of 3-D imaging using a swept 1-D array transducer on the evaluation of TAC metrics and the effect of transducer motion in combination with flow on 3-D parametric maps generated using both plane wave imaging (PWI) (seven angles) and focused imaging (FI). Correlation maps were introduced to evaluate the spatial blurring of TAC metrics. A research ultrasound scanner and a pulse-inversion algorithm were used to obtain DCE-US. The 2-D (frame rate 10 Hz) and 3-D (volume rate 0.4 Hz) images were acquired of a simple wall-less vessel phantom (flow phantom) and a cartridge phantom. Volumetric imaging provided similar TACs to that of the higher 2-D sampling rate. Varying sweep speed and acceleration/deceleration had little influence on the 3-D TAC compared to 2-D for both FI and PWI. Sweeping motion and limited temporal sampling (0.4 Hz) did not change the spatial correlation of TAC metrics measured using FI, whereas a small increase in correlation across the cartridge phantom was observed for PWI. This was attributed to grating lobe artifacts, broad beam spatial blurring, and incoherent compounding caused by motion. Increased correlation will reduce the spatial resolution with which inhomogeneity of vascular perfusion can be mapped supporting the choice of FI for DCE-US.**

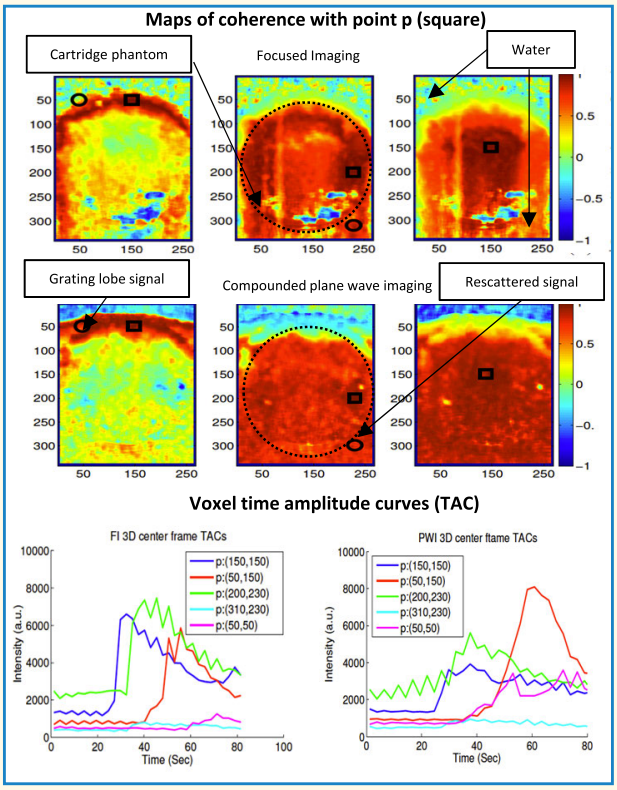

***Index Terms*—3-D dynamic contrast-enhanced ultrasound imaging (DCE-US), correlation map, parametric imaging, time–amplitude curve (TAC).**

Manuscript received 8 February 2023; accepted 11 April 2023. Date of publication 17 April 2023; date of current version 28 June 2023. This work was supported in part by the Cancer Research U.K. under Program C20892/A23557 and in part by the National Health Service (NHS) funding to the National Institute of Health Research (NIHR) Biomedical Research Center at The Royal Marsden and The Institute of Cancer Research. *(Corresponding author: Elahe Moghimirad.)*

Elahe Moghimirad, Jeffrey Bamber, and Emma Harris are with the Joint Department of Physics and the CRUK Cancer Imaging Center, The Institute of Cancer Research, SM2 5NG London, U.K., and also with the Royal Marsden NHS Foundation Trust, SM2 5PT London, U.K. (e-mail: elahe.moghimirad@gmail.com; emma.Harris@icr.ac.uk).

Zhiting Xu and Hong Ding are with the Department of Ultrasound, Huashan Hospital, Fudan University, Shanghai 200040, China.

This article has supplementary downloadable material available at https://doi.org/10.1109/TUFFC.2023.3268009, provided by the authors.

Digital Object Identifier 10.1109/TUFFC.2023.3268009

I. Introduction

CHANGES in tumor blood perfusion, which can be detected as early as one or two weeks after the start of therapy, have been shown to differentiate between tumors that do or do not respond to chemoradiation [1], [2]. This is a much shorter time in comparison to the time it takes for reliable changes in tumor-size-based biomarkers to be detected by conventional imaging methods, such as CT and MRI. Studies have shown that assessing the tumor size by morphological measurement could result in over- or underestimating the tumor response to chemotherapy [3], [4] and that the early response of tumors to therapy is difficult to assess using conventional radiographic modalities [5]. In a preclinical

Highlights

- **For low volume-rates (0.4 Hz), swept array acquisitions provided good estimates of (tumour-mimicking) contrast flow dynamics within a volume of interest.**
- **Novel aspects of this work include the investigation of how probe motion, contrast signal scattering and grating lobes influence volumetric parametric imaging (VPI).**
- **VPI using plane wave imaging is subject to small increases in signal coherence across the image due to grating lobes and rescattering reducing ability to detect spatial heterogeneity in flow dynamics.**

setting [6], it was shown that contrast ultrasound (CEUS) demonstrated a reduction of tumor perfusion 2 days after treatment which was 4 days before the difference of tumor sizes became measurable by conventional imaging. Accurate and reproducible techniques to assess changes in tumor vascularity, and therefore tumor response, may be a potential way to improve how we treat patients [7]. Longitudinal studies of the tumor response could involve numerous measurements, ideally before and after each treatment and during follow-up. Ultrasound, which is a safe and low-cost imaging modality, can be conveniently used at the patient bedside, or in the therapy clinic, and therefore is a perfect tool for this purpose. Dynamic contrast-enhanced ultrasound imaging (DCE-US) can be used to interrogate tumor vasculature and metrics derived from the time–amplitude curve (TAC), which may be useful prognostic and predictive biomarkers of early tumor response to therapy [8]. Such imaging biomarkers are attractive in that they can provide spatial and temporal evaluations of response [9], [10]. Spatially, parametric maps of TAC metrics can be generated, which map tumor vascular heterogeneity and heterogeneity of response [11]. It can be valuable to assess the tumor response for subregions based on the change in TAC characteristics in longitudinal studies. This can be used to characterize different parts of the tumor separately and to detect the well-vascularized versus poor-vascularized areas and this provides scope to spatially adjust targeted cancer therapies, such as radiotherapy, based on the observed heterogeneity of response, using, for example, intensity modulated radiotherapy [12]. Texture features of the parametric images can also be introduced to characterize vascular heterogeneity as a biomarker in its own right [13].

It is expected that a 3-D DCE-US imaging system will both provide the opportunity to image the entire tumor, enabling tumor heterogeneity of response to be explored, and offer the greatest reproducibility by overcoming variations in plane selection associated with 2-D imaging [14], [15], [16], [17]. Ideally, DCE-US requires high ($>$10 Hz) temporal resolution to sample the TAC, i.e., at the volume rates typically afforded by 2-D matrix arrays; however, these are not always available. The alternative is a continuously swept linear array transducer, which is used in most 3-D clinical probes and can be considered more practical to implement clinically. Therefore, this was the setup considered in the current article. These probes, however, operate at slower sweep speeds, from less than 1 Hz to up to $\sim$10 Hz which may not be adequate to temporally sample the dynamics of the contrast signal.

In terms of the volume rate achievable with swept array transducers, plane wave imaging (PWI) may offer advantages over focused imaging (FI). The requirement for adequate temporal sampling of TAC may mean that high volume rates are required, i.e., volume rates that approach the typical imaging frame rates which are used in 2-D DCE-US imaging. Swept array probes with a volume rate of 10 Hz may be adequate; however, FI frame rates may limit the elevational spatial sampling distance and/or the volume of interest (VOI) that can be imaged. For example, for a 128-element transducer (128 lines) with imaging depth of 10 cm, the maximum frame rate is 60 frames/s. For non-linear contrast mode imaging, where at least two pulses are required per line, the maximum frame rate reduces to 30 frames/s. For a volume rate of 10 Hz (0.1 s per sweep), the elevational dimension of the VOI would only be sampled with three frames. Even for a modest sweep distance of 20 mm traversed by the probe in 0.1 s, the elevational spatial sampling would be poor with $\sim$7 mm between frames. To improve the elevational spatial sampling, the VOI (imaging depth, sweep distance, and lateral imaging width) or lateral spatial sampling would need to be reduced.

In our previous work [10], we evaluated PWI and FI in 2-D DCE-US using a flow phantom. The study showed that both PWI and FI can suffer from motion artifacts where the pulse inversion algorithm has a false increase of signal between the positive and negative pulses due to target (microbubbles) motion. In addition, for PWI only, a motion artifact can also be generated by incoherent summation between the compounding angles which resulted in a reduction of contrast signal. Considering this, it is possible that introducing a swept array transducers for 3-D DCE-US can lead to more artifacts due to the relative motion of the transducer between the pulses and the compounding angles which is studied in this article.

Another source of artifact for PWI was observed to be high-frequency grating lobe artifacts [9] caused by harmonics of the contrast signal. Mapping the spatial correlation between the pixels within parametric maps revealed that grating lobes from the contrast signals in one region of a phantom influence the contrast signals (and therefore TAC parameters) in other parts of the phantom [11]. Correlation between TAC in different pixels was greater for PWI, suggesting that the ability to discern spatial heterogeneity of TAC (i.e., perfusion characteristics) within tumors would be reduced for PWI compared to FI. It is therefore instructive to evaluate and compare 3-D parametric

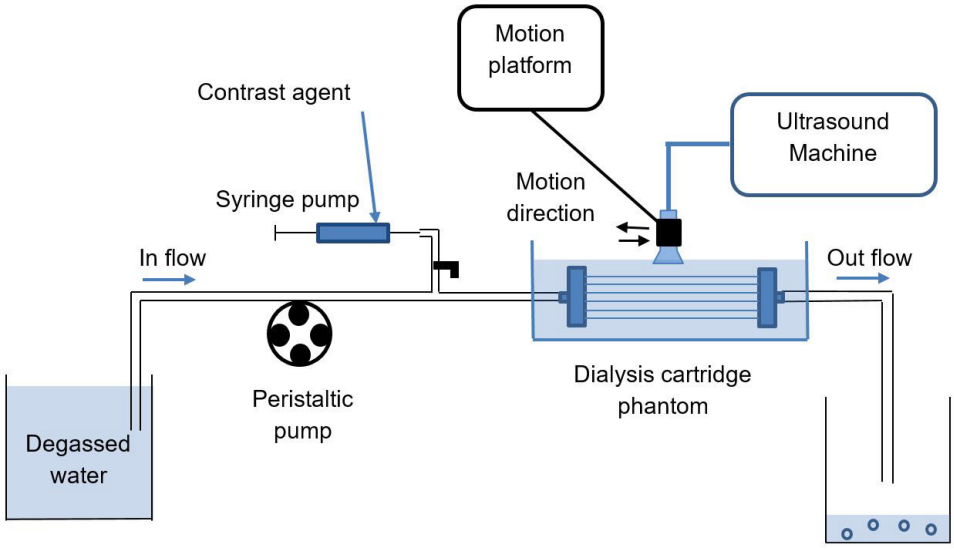

Fig. 1. Phantom setup composed of a dialysis cartridge connected to a peristaltic pump and an injection pump to inject the contrast agent through the system (the mixed fluid of water and contrast agent was removed from the system after passing through the cartridge).

maps generated using a swept array probe with both FI and PWI to understand the advantages and disadvantages of both methods.

The aim of this work was to understand the effect of lower temporal sampling (i.e., <1 Hz) on the TAC curves and to evaluate the effect of transducer motion on 3-D parametric maps generated using PWI and FI by examining maps of the spatial correlation across parametric maps. To achieve this, a single vessel phantom (flow phantom) and a microvessel phantom were imaged by sweeping a 1-D array transducer back and forth in a configuration chosen so that appearance of the phantoms was homogeneous in the elevational direction, i.e., there was minimal interplane TAC variation. This approach enabled evaluation of the effect of probe motion on the spatial distribution of TAC parameters, without the potential to mix different flow patterns from multiple planes.

II. Materials and Methods

A dialysis cartridge and a tissue-mimicking flow phantom were used in this study to perform different experiments. The dialysis cartridge was composed of ~100 000 parallel microtubes, each 200 μm diameter. The flow phantom was model 524 (ATS Laboratories Inc., Norfolk, VA, USA) with 0.5 dB/cm/MHz attenuation coefficient and four different vessel diameters. The 4-mm-diameter vessel located 15 mm below the scan surface surrounded by tissue-mimicking media (resulting in a homogenous speckle pattern) was used in this study as a relatively easy-to-interpret arrangement to confirm the presence of grating lobes and rescattering of ultrasound signal and their influence on parametric maps. Both phantoms were connected to an H.R. flow inducer MHRE 200–250 v peristaltic pump (Watson Marlow Ltd., Falmouth, Cornwall, U.K.) as shown in Fig. 1 (the cartridge phantom was replaced by the flow phantom in the second setup). A constant flow of 1 ml/s equilibrated gas saturated water [18] was maintained through the system while a 0.4 ml of contrast agent (Sonazoid[1]; GE Healthcare, Oslo, Norway) was injected at 3.18 ml/min using NE-1010 injection pump (New Era Pump Systems Inc., Farmingdale, NY, USA). Constant flow of 1 ml/s was chosen to provide approximately 0.3 mm/s flow speed in the microtubes similar to the flow speed in capillaries [19].

A Vantage[1] system (Verasonics Inc., Kirkland, WA, USA) connected to an ATL L7-4 linear transducer (Philips Healthcare, Cambridge, MA, USA) was used to obtain DCE-US images reconstructed using a two-pulse pulse-inversion algorithm to generate a microbubble-specific echo signal [20]. The pulse intervals were chosen to be 150 μs (based on the previous study [10]) covering more than the intended imaging depth to reduce the rescattering of sound from inside the cartridge and the bottom of the phantom. In addition, using a pulse interval of 150 μs provides a maximum imaging depth of ~11.5 cm, which more closely mimics the clinical scenario where imaging depths will typically be greater than the 5 cm needed to image the phantoms in this study. Minimum 800 frames were acquired at 10 Hz, for both FI and PWI, corresponding to 80 s of TAC starting from injection. This was enough time to cover the full wash-in and a part of wash-out period. FI was composed of 128 focused beamlines acquired with 300 μs (=2 × pulse interval) line intervals and was recorded at 10 Hz frame rate. Maintaining the 10 Hz frame rate for PWI and compounding angle intervals of 300 μs, seven angles tilted from $-10°$ to $+10°$ were compounded to generate the PWI DCE-US images. FI and PWI parameters were chosen based on the previous studies so that they have similar contrast and microbubble disruption rate determined using a simple single-vessel flow phantom [10]. The parameters were focal depth (FD) = 20 mm (for FI), F-number = 4, mechanical index (MI) = 0.15, transmit frequency = 4 MHz, and number of angles (NA) = 7 (for PWI).

A. Effect of Low Temporal Sampling on TAC

The first experiment with the cartridge phantom was used to determine if TAC from volumetric data acquired at a low volume rate (0.4 Hz) provides similar TACs from a VOI and regions of interest (ROI) within that volume. The 2-D

[1]Trademarked.

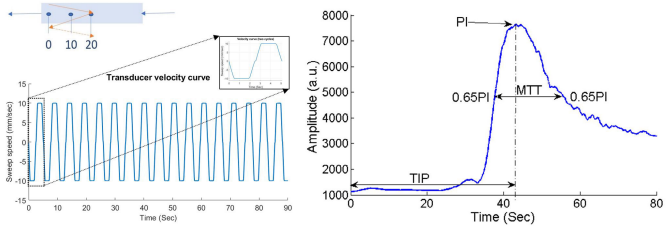

Fig. 2. (a) Three positions marked at 0, 10, and 20 mm along the phantom and the 3-D volumetric motion profile. (b) Schematic to illustrate PI, MTT, and TIP parameters extracted from TACs.

DCE-US imaging of the cartridge phantom was acquired at three positions along the length of the cartridge phantom with the probe stationary. The 3-D DCE-US imaging was acquired with the probe sweeping out a volume 20 mm in length (volumetric imaging). The probe was moved back and forth with the motion and speed profiles illustrated in Fig. 2. TACs from volumetric imaging were generated in two ways to give 3-D TACs and volumetric TACs. Details of the different TACs are as follows.

1) *2-D TAC:* This is acquired with the probe stationary and sampled at 10 Hz (the 2-D frame rate) [Fig. 3(a)]. The samples were simply connected, and the curve was slightly smoothed without using any curve fitting method to avoid introducing the fitting error. This TAC represents the contrast dynamics in a 2-D ROI for a single image plane. The 2-D TACs were generated for three different planes p0, p10, and p20 corresponding to the transducer located at 0, 10, and 20 mm, respectively.
2) *3-D TAC:* This is acquired with the probe sweeping between p0 and p20, and slices of the phantom were sampled at 10 Hz shown as the dotted line sections in Fig. 3(b) (left). It should be noted that this is the contrast dynamics of multiple planes across the imaging volume. The 3-D TAC was the curve fitted to these samples and shown as the dotted line in Fig. 3(b) (right). Due to the low sampling rate of 3-D TAC, a smoothing spline fitting curve was used to smooth the curve with minimum fitting error.
3) *Volumetric TAC:* All the image planes in one sweep were averaged to form one single VOI. Each sweep between p0 and p20 gives one volumetric image sampling the whole VOI at 0.4 Hz. This represents the contrast dynamics averaged across the whole VOI. The TAC was calculated from this low temporally sampled volume Fig. 3(c) (right).
4) p0 (3-D), p20 (3-D) plane, and central plane (3-D) TACs: These are acquired with the probe sweeping between p0 and p20 and represent the contrast dynamics of a single ROI in the plane positioned at p0, p20, and p10, respectively. TACs were a plot of the mean contrast signal in the ROI sampled at 0.4 Hz, while the probe was moving at 0 mm/s for p0 and p20 and 10 mm/s for the central plane TAC. The data points were swept to find the central planes, p0 and p20 with the same resulting volume rate.

B. Effect of Varying Transducer Motion Parameters on TAC

A second experiment compared the effect of varying acceleration/deceleration on 3-D TACs with constant sweep speed for FI and PWI. Volumetric imaging of a volume 20 mm in length was acquired using PWI and FI sweeping with maximum speeds of 10 mm/s and acceleration/deceleration of 10, 20, and 50 mm/s^2. Next, the acceleration was kept constant at 20 mm/s^2 and the sweep speed was changed to 10 and 20 mm/s, corresponding to volume rates of ∼0.4 and ∼0.5 Hz. The experimental setup limited the maximum volume rate due to the creation of surface waves in the tank. For these data, 3-D TACs were compared to TACs generated from single planes acquired during volumetric imaging at the same three positions along the phantom that were used for 2-D DCE-US imaging.

C. Effect of Transducer Motion on Parametric Imaging

For the maximum sweep speed of 10 mm/s and acceleration/deceleration of 20 mm/s^2, a 3-D structure of data was recorded consisting an 80 s TAC for each pixel [see Fig. 3(d)] in the image plane corresponding to 800 frames with temporal sampling of 10 Hz for FI and PWI. The TACs were then averaged over 11 × 11 square pixels (∼1 × 1 mm) in the image plane to reduce noise. Parametric maps were formed for three metrics: peak intensity (PI), time from injection to peak (TIP), and mean transit time (MTT). MTT was calculated as the time between 65% of PI in the wash-in phase and the 65% of PI in the wash-out [see Fig. 2(b)]. Parametric maps were then compared for 2-D TAC versus central plane (3-D) TAC for FI and PWI. The 3-D center plane was referred to the plane where the transducer speed was at a maximum (10 mm/s) in both sweep directions. To find the position of the center plane, first the times/planes were calculated for p0's and p20's corresponding to zero sweep speed on the sweep speed curve. Then, the mean of those was assigned to the 3-D center plane.

Aiming to detect the effect of grating lobes on the spatial distribution of the contrast signal in different parts of the phantom in the scan plane, a TAC similarity measure was defined for each pair of pixels [10]. Each pixel in the imaging plane has an associated TAC, so the reference TAC was defined as the TAC of a chosen reference pixel. The correlation coefficient was then calculated between the reference TAC and the TAC that corresponds to each of the pixels in the imaging plane (Fig. 4) and assigned to that pixel in the correlation map.

Three reference points were chosen to sample all the dominant temporal patterns of TAC (i.e., TAC shape) observed in the phantom at p:(row, column): p1:(50,150), p2:(200,230), p3:(150,150). The corresponding correlation maps and a histogram of all the points in those maps were then used to compare the imaging modes. TACs were also compared for these points plus some extra points at p4:(310,230) and p5:(50,50) to further study the signal in different parts of the phantom, in particular to examine the rescattering of contrast signal, which may occur in addition to grating lobe artifacts [10].

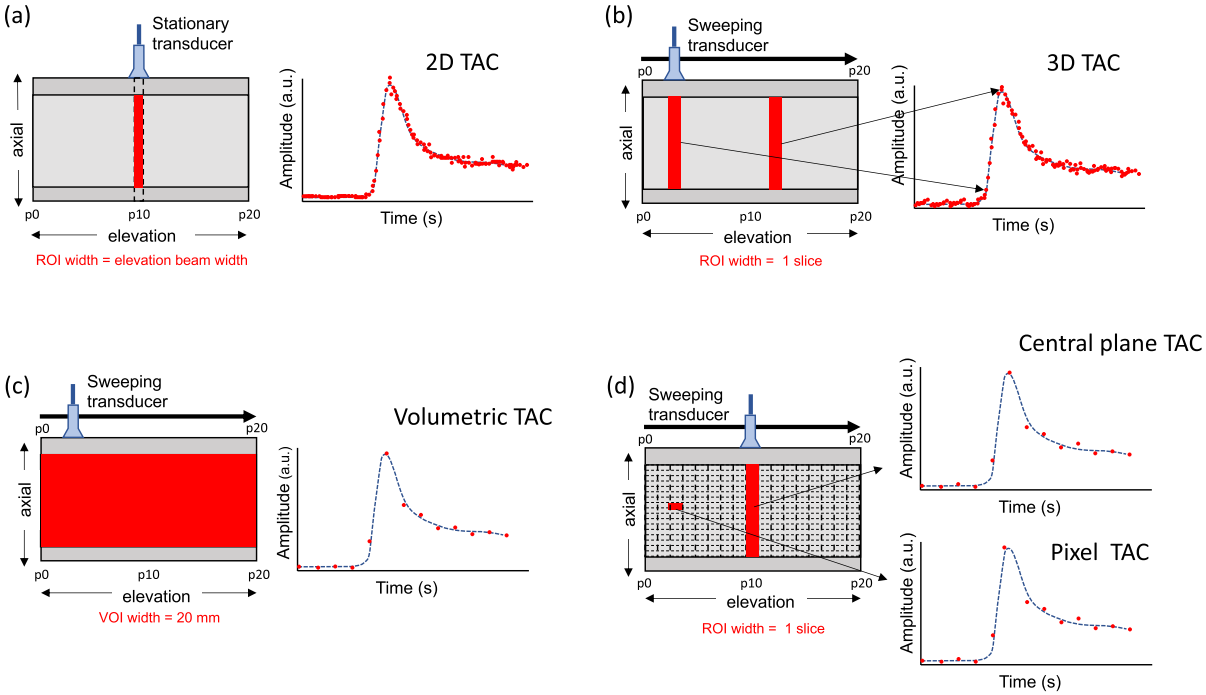

Fig. 3. Schematic illustrating the formation of (a) 2-D TAC, (b) 3-D TAC, (c) volumetric TAC, and (d) central plane and pixel TACs, which are described in the text. The elevational-axial plane of the phantom is shown on the left of each panel. The elevational dimensions of the different analysis regions or volumes used to generate data points that form the TAC are shown in red. The term ROI is used to remind the reader that the data are from one imaging plane only. In reality, due to the finite elevational beamwidth, 2-D TAC used data averaged over a volume of data with elevational dimension equal to the elevational beamwidth. Similarly, plane TACs and pixels TACs used data from ROIs with elevational width due to the elevational beamwidth plus additional width due to transducer motion; we refer to this as the slice width. Note that the transducer sweeps from p0 to p20, then from p20 to p0, and so on; therefore, alternating data points in (c) and (d) are for sweeps in opposing directions. For (b), the direction of the transducer changes every 25 data points in the 3-D TAC.

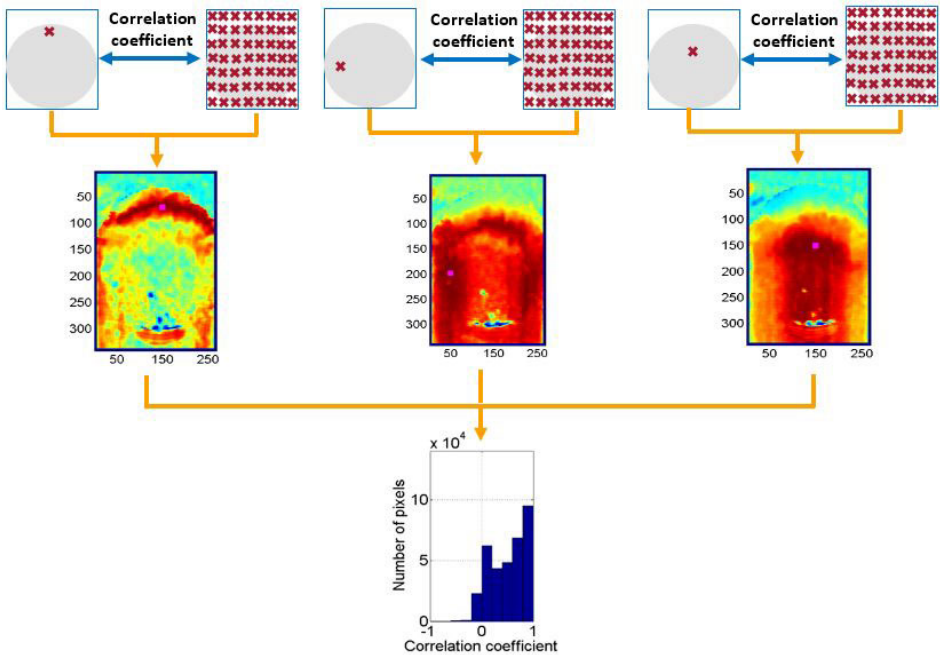

Fig. 4. Correlation maps of the TACs produced for three reference points and their overall (combined) histogram.

Rescattering of the contrast signal occurs when a strong signal passing through the medium/phantom gets reflected one or more times after the initial echo.

Similar evaluation was performed for the flow phantom with two reference points at p:(row, column): p1:(110,135), and p2:(100,230) one of which is in the water/background and one in the vessel to evaluate the grating lobe effects and the vessel pixels. The TACs for these points plus p3:(175,135) were compared for more evaluation of the actual signals, grating lobe artifacts, and the rescattering effect.

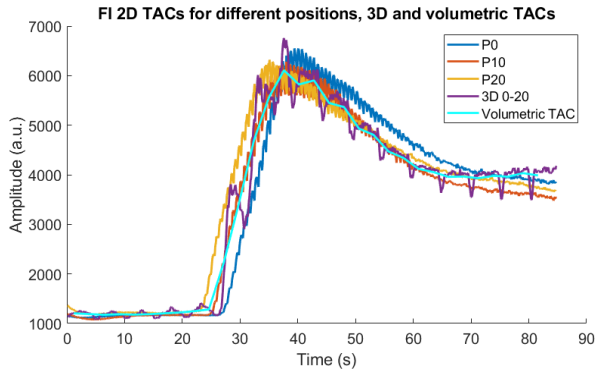

Fig. 5. Cartridge phantom: representative 2-D TACs for positions 0, 10, and 20 compared to the 3-D and volumetric TACs.

III. Results

Fig. 5 shows example 2-D TACs acquired at positions 0, 10, and 20 mm, the 3-D TAC, and the volumetric TAC. The peaks of the 2-D TACs are similar, with variation between peak amplitude falling within the expected experimental uncertainty $\sim+/-7\%$ (standard deviation measured over three repeat experiments). There was no observed trend in PI with position along the phantom. The arrival times were different. As expected, contrast agent arrived sooner at p20, which was closer to the water inlet, then p10 and then p0. The 3-D TACs from all frames during volumetric imaging showed amplitude variations (ripples) with the same frequency as the volume rate. During the wash-in phase of the TACs, periodic amplitude minimums are similar to the amplitude of the 2-D TACs at p0 and the maximums are similar to the amplitude of the 2-D TACs at p20. This then changes after the peak where the minimums correspond to p20 and vice versa. From Fig. 5, we also observe that the volumetric TAC provides a good estimation of the TAC despite the lower sampling rate; averaging over the whole VOI provides a smoother TAC; however, all information on any spatial heterogeneity of contrast dynamics is lost using this approach.

This is further studied in Fig. 6 for 10 mm/s sweep speed and varying acceleration/deceleration. The results were similar for acceleration/deceleration of 20 mm/s^2 and 10 mm/s^2. When the acceleration/deceleration was increased to 50 mm/s^2, these extremums occurred at the p0/p20 plus acceleration time which could be due to the artifacts from vibration of the probe due to motion becoming less smooth. The ripples were also seen to increase in amplitude when the acceleration/deceleration was increased to 50 mm/s^2.

Fig. 7 shows representative 3-D TACs for FI and PWI for different sweep speeds (with constant acceleration/deceleration $=$ 20 mm/s^2), and variation between them was again within expected variation between repeat measurements. There was little effect of sweep speed and variation between the 3-D TAC. There was no apparent trend in TAC curves with volume. The small shift in arrival time is due to the fact that 3-D TAC is actually a spatial distribution of pixel intensity along the phantom (back and forth) and so a certain time from injection may correspond to different imaging plane when using different sweep speeds. The shape of the 3-D TACs varied between PWI and FI, with FI 3-D TAC appearing to have a narrower peak than PWI 3-D TAC.

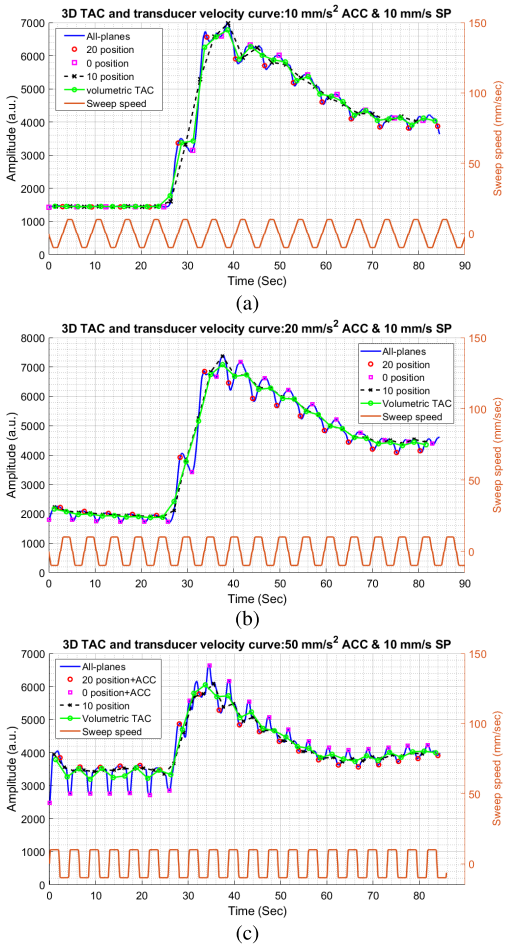

Fig. 6. Cartridge phantom: 3-D TACs compared to the p0 (3-D), p20 (3-D), and central plane (3-D) TAC data extracted from 3-D DCE-US data recorded while the transducer is moving and the corresponding sweep speed curve for (a) 10 mm/s^2 acceleration/deceleration, (b) 20 mm/s^2 acceleration/deceleration, and (c) 50 mm/s^2 acceleration/deceleration.

Parametric images of FI for 2-D and central plane (3-D) TACs are compared in Fig. 8 to evaluate the effect of movement and downsampling. The corresponding correlation maps are also shown in Fig. 9. Figs. 10 and 11 also show parametric images and coherence maps for PWI. The coherence maps reveal inhomogeneity in the phantom which is consistent with the design of the cartridge. Fluid flows through the center of the phantom first and at a greater speed as the inlet is centrally positioned. A video of the contrast flowing into the phantom is included in the Supplementary Material. Only 45 s of the TAC is shown in the video with three times increased frame rate for illustration purpose. The pattern of PI can be explained by the combination of a greater concentration of microbubbles flowing through the center due to the proximity of the inlet and attenuation of contrast signal by shallower regions of the phantom. The 2-D versus central plane (3-D) correlation maps for cartridge are similar showing that sweeping and under sampling of the TAC do not increase correlation for FI. The TACs show the rescattered signal at p:(310,230) being similar to that of p:(200,230) in terms of arrival time but with much less PI as expected. There is no signal in the background at p:(50,50)

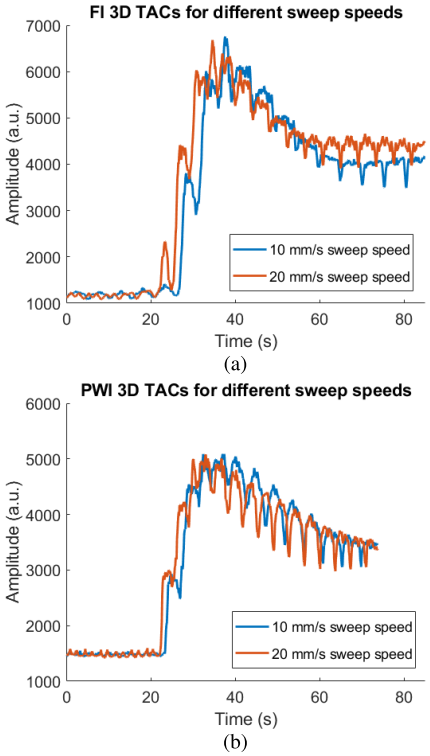

Fig. 7. Cartridge phantom: 3-D TAC curves for two different sweep speeds: 10 and 20 mm/s with constant acceleration/deceleration of 20 mm/s^2 for (a) FI and (b) PWI.

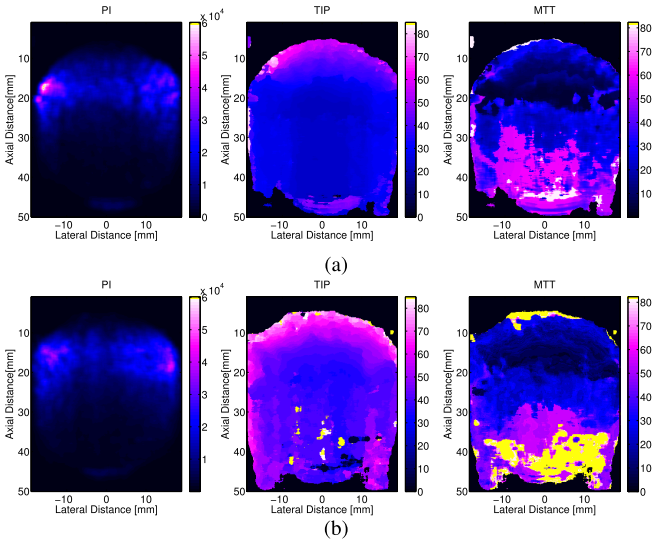

Fig. 8. Cartridge phantom: parametric maps for PI, TIP, and MTT (from left to right) for (a) 2-D FI and (b) 3-D central plane FI.

for 2-D FI whereas there is a slight increase in the TAC for central plane (3-D). Please note that this signal is not similar to that of p:(50, 150) as is for PWI (Fig. 11) and so cannot be due to grating lobes.

In Fig. 10, there is evidence of contrast signal external to the phantom which was previously attributed to high-frequency grating lobes [9].

For PWI, the 2-D and central plane (3-D) correlation maps and their corresponding histograms are not similar, suggesting that PWI is affected by sweeping motion. The high-correlation areas are much more extended for central plane (3-D) correlation map [Fig. 11(b)] in comparison to 2-D central plane correlation map [Fig. 11(a)] for the reference point at (150,150). For the PWI correlation map, when the reference point is at the top of the phantom at (50,150), some high-correlation pixels appear in the water surrounding the phantom which is probably caused by high-frequency grating lobes generated by harmonics of contrast signal. The TACs shown for different points show the similarity of the arrival time for p:(50,150) and p:(50,50) supporting the above-mentioned hypothesis. However, a rise in the PWI central plane (3-D) TAC for (50,50) at around 60 s as opposed to the 2-D TAC may be due to bubble formation in the tank due to the repetitive motion of the probe. Also, small amounts of bubbles that have leaked from the phantom maybe set in motion by the moving phantom and hence contribute to the background contrast signal.

TABLE I
CARTRIDGE PHANTOM: CONTRAST FOR 3-D CENTER PLANE FI AND PWI FOR THREE MEASURES

	FI 1	FI 2	FI 3	PWI 1	PWI 2	PWI 3
ContrastRatio	0.91	0.94	0.93	0.53	0.54	0.47

The contrast ratio of the whole cartridge region to the background was also calculated using

$$\text{contrastRatio} = \log\left(\frac{\text{meanPI\_cartridge}}{\text{meanPI\_background}}\right)$$

where meanPI corresponds to the average PI. The ROI used for calculation covered the whole area of the phantom for the cartridge area and the rest of the pixels for background. The corresponding contrast ratios are shown in Table I comparing 3-D center plane FI and PWI for three repeats.

To further investigate the effect of motion on the gratings lobes, we employed a simple wall-less vessel phantom (flow phantom). The parametric and correlation maps are similarly evaluated for FI in Figs. 12 and 13 and PWI in Figs. 14 and 15. The TAC is much sharper around the center compared to periphery, as microbubbles are injected with a syringe through a valve with a speed much higher than the background flow speed (3.18 ml/min microbubble through a very small cross section of a syringe compared to 1 ml/s peristaltic flow through the vessel cross section). Hence, they arrive at the center of the vessel first with a very high concentration and then spread out. This results in a sharper TAC around the center and consequently a smaller MTT. In FI correlation maps, the background appeared noisier for central plane (3-D) compared to 2-D DCE-US possibly due to downsampling and thus a loss of high-frequency information in the TAC. The grating lobes appear in the PWI parametric images (Fig. 14) as two wings on the side of the vessel with a high correlation to the vessel pixels as shown in the correlation maps (Fig. 15). Looking at the TACs for p:(175,135), the rescattered signal is of a very small PI compared to the actual vessel signal at p:(110,135) and is negligible. There is no signal at p:(100,250) for FI, whereas it is comparable to the vessel signal for PWI.

IV. DISCUSSION

Here, we used a cartridge phantom which was homogeneous in the sweep (elevational) direction to evaluate the 3-D TACs

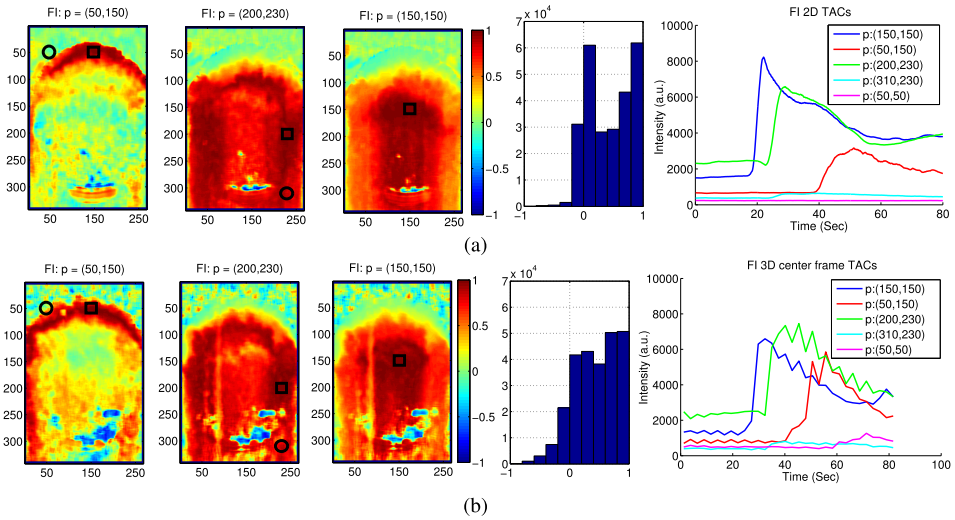

Fig. 9. Cartridge phantom: correlation maps for three reference points at (row, column) (from left to right): p1:(50,150), p2:(200,230), and p3:(150,150) marked as black squares in each panel, and their combined histogram and the corresponding TACs plus two extra points at p4:(50,50) and p5:(310,230) marked as black circles for (a) 2-D FI and (b) central plane (3-D) FI.

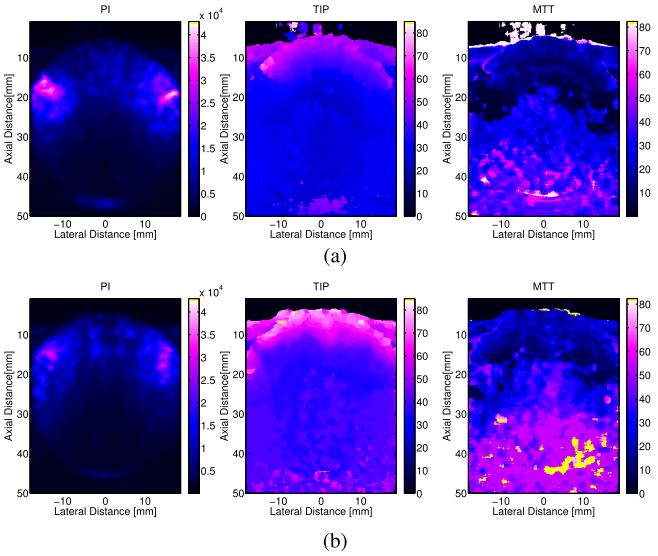

Fig. 10. Cartridge phantom: parametric maps for PI, TIP, and MTT (from left to right) for (a) 2-D PWI and (b) 3-D central plane PWI.

TABLE II
PI, TIP, AND MTT FOR 2-D FI AND CENTRAL PLANE (3-D) FI FOR THREE MEASURES

	2D 1	2D 2	2D 3	3D 1	3D 2	3D 3
PI	6909	6365	6430	6523	7375	6394
TIP	39.4	34.5	38.0	37.6	37.6	37.6
MTT	22.8	34.8	28.6	35.0	34.0	36.0

for different sweep speeds for FI and PWI. Homogeneity was confirmed by visual comparison of the 2-D parametric maps (not shown) and the TACs acquired at three different positions along the transducer moving axis using a big ROI covering the whole phantom cross section (Fig. 5). The dialysis cartridge and flow rate were chosen to mimic a TAC (averaged over an ROI which encompasses the entire phantom in a 2-D plane) typical of that would be expected for a tumor [21]. Fig. 5 shows that volumetric TACs sampled at 0.4 Hz which was significantly lower than rates typically used for 2-D DCE-US provide similar TAC information to that of the higher 2-D sampling rate used in this work (10 Hz). There was a small reduction in the PI of the volumetric TAC compared to 2-D and 3-D TACs which can be expected, because the volumetric TAC averages contrast signal over time and the PI occurs at different times along the length of the phantom (in the sweep direction). This approach may be suitable if information on tumor heterogeneity is not required. It should be noted however that the volumetric TAC may not be suitable for flow dynamics with higher frequency components, i.e., shorter time to peaks or shorter wash-out times, where the greater temporal averaging of the volumetric TAC may significantly reduce PI.

There were no notable differences between the 2-D TAC acquired at p10 when the probe was stationary compared to that of the estimated p10 frame in the 3-D TAC, an example of which can be seen in Fig. 6 in dotted line. It should be noted that the volume of the phantom represented by the p10 ROI for the sweeping probe will be slightly different to that when the probe is stationary, i.e., during the time taken to acquire one frame, the probe moves 1 mm. The effect of this is minimized because of the homogenous nature of the phantom in the sweep direction, allowing us to compare the stationary and moving cases. From these data, it is shown that TACs within individual slices of the volume are adequately sampled at sampling rates as low as 0.4 Hz. This implies that if we used the volumetric data to form 3-D parametric maps of TAC metrics of individual voxels (with elevational dimension equal to as a 2-D image slice width), the information would be representative of the blood flow within that VOI. This is shown in Fig. 8, in which mean PI, TIP, and MTT for the central 3-D plane are within the measured variation between repeat injections for 2-D (Table II).

For both FI and PWI, varying sweep speed and acceleration/deceleration had little effect on the shape and parameters of the 3-D TAC (Figs. 6 and 7). We primarily attribute the ripples in the 3-D TAC due to the differences in microbubble arrival time along the length of the phantom. For FI, as relative motion between target and transducer increases, an increase

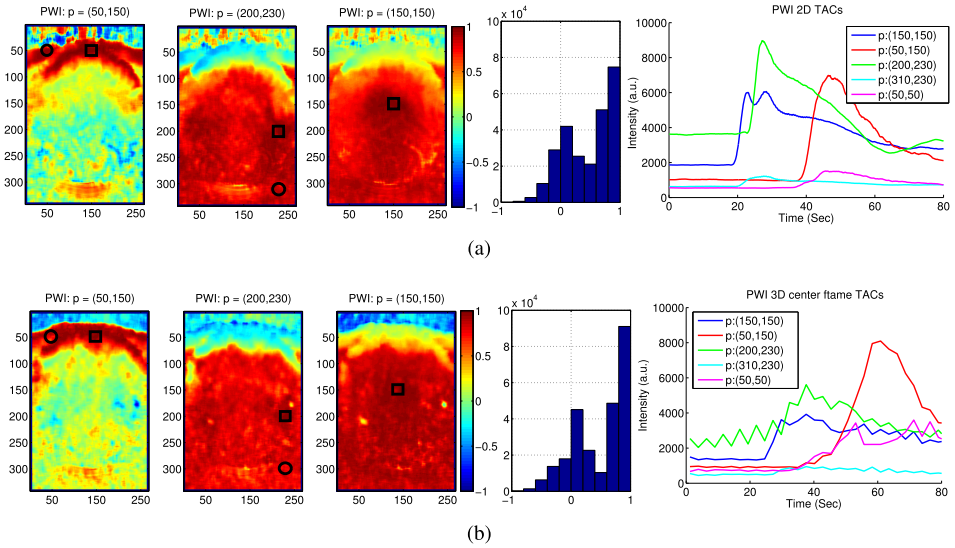

Fig. 11. Cartridge phantom: correlation maps for three reference points at (row, column) (from left to right): p1:(50,150), p2:(200,230), and p3:(150,150) marked as black squares in each panel, and their combined histogram and the corresponding TACs plus two extra points at p4:(50,50) and p5:(310,230) marked as black circles for (a) 2-D PWI and (b) central plane (3-D) PWI.

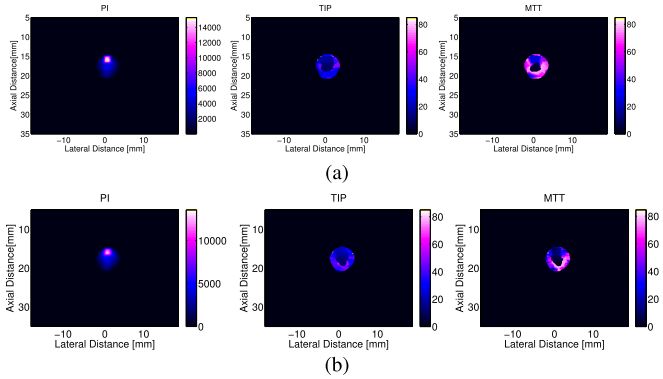

Fig. 12. Flow phantom: parametric maps of the flow phantom for PI, TIP, and MTT (from left to right) for (a) 2-D FI and (b) FI central plane (3-D).

in signal occurs due to target motion between positive and negative pulses, a type of flash artifact [10]. A probe speed of 20 mm/s retrograde to the flow (∼7 mm/s) gives a relative speed of ∼27 mm/s, which would result in ∼1 dB increase in contrast signal. Also, for PWI, at 27 mm/s, ∼1 dB loss in signal could be expected due to loss of coherence between compounding angles [10], [22], [23] which was not detectable in the 3-D TAC due to the large variation signal due to the variation in the arrival times along the phantom (∼10%–20%). As a volume rate of 0.4 Hz provides adequate sampling of TAC typical for tumor studies with DCE-US, it is unlikely that much higher sweep speeds are required and therefore these motion artifacts will be small. Furthermore, greater sampling rates will require greater speeds; the size of an imaging voxel will be increased at greater sweep speeds leading to degradation of the spatial resolution in the elevational direction.

The comparisons of 2-D and 3-D TACs presented here have not been previously reported. Mahoney et al. [24] used 3-D DCE-US to image the flow of contrast through a flow phantom using a swept array transducer with a volume rate of 1.6 volumes per second; however, they did not study the effect of using this low volume rate on their TAC nor did they compare 3-D TAC to 2-D TAC. A recent study by Ruan et al. [25] compared the variability of the average PI measured in five flow phantoms using 2-D and 3-D CEUS acquired at 10 and 1.5 Hz, respectively. The study found that measurements of the average PI made with 3-D CEUS had smaller coefficient of variation across repeat measurements. TACs were not evaluated, and direct comparison of average PI measured using 2-D and 3-D was not possible as the most of the phantoms were not homogenous in the elevational direction.

The differences in the TAC shape for FI and PWI were observed previously for 2-D TAC [9], [10], [11] and were attributed to: 1) the wider lateral beamwidth of PWI which can result in spatial blurring of signal; 2) target (microbubbles) movement between the compounding angles resulting in failure of synthetic focusing for PWI; and 3) high-frequency grating lobe artifacts originating from high-frequency component of the contrast signal (observed previously in [10]).

Parametric images were formed for three different metrics—PI, TIP, and MTT—to evaluate the spatial heterogeneity of the flow, specifically the spatial blurring of the contrast signal from one area of the phantom to another for 3-D imaging using FI and PWI. Here, we sample the central plane of voxels within a 3-D volume [central plane (3-D)], with elevational dimension of the voxels equal to the elevational beamwidth and the distance the probe travels during the time it takes to acquire one image frame. The comparison of parametric images and their corresponding correlation maps for a central plane in the 3-D volume obtained using 3-D DCE-US and those obtained using 2-D DCE-US (Figs. 8–11) showed that the sweeping motion of the transducer and limited temporal sampling of the TAC (0.4 Hz) did not change the correlation of FI TAC data across the phantom but a small increase in correlation, i.e., signal blurring, was observed for PWI. In general, PWI had increased correlation across the cartridge phantom compared to FI (compare Figs. 9 and 11) which was expected due to previously observed grating lobe artifacts

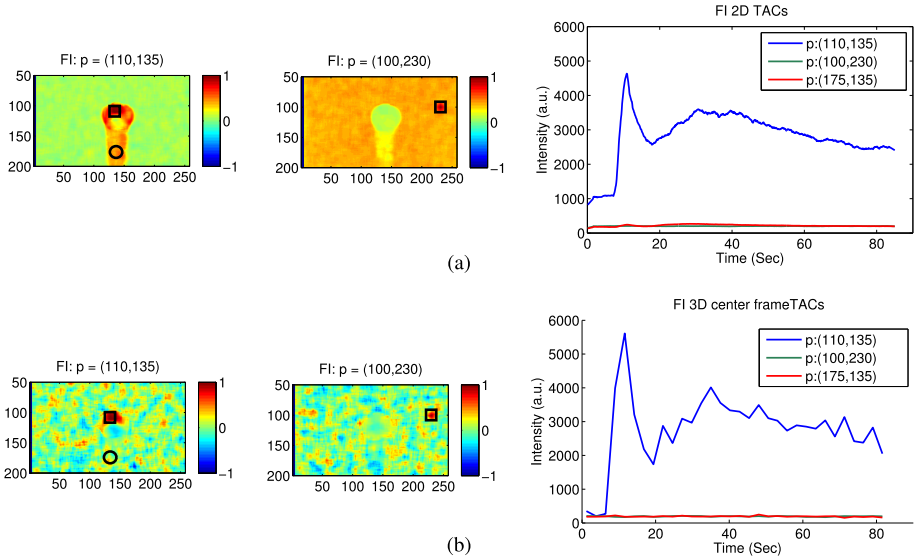

Fig. 13. Flow phantom: correlation maps for two reference points at (row, column) (from left to right): p1:(110,135) and p2:(100,230) marked as black squares in each panel and their corresponding TACs in addition to the TAC for p3:(175,135) (marked as black circle) for (a) 2-D FI and (b) 3-D FI for center plane.

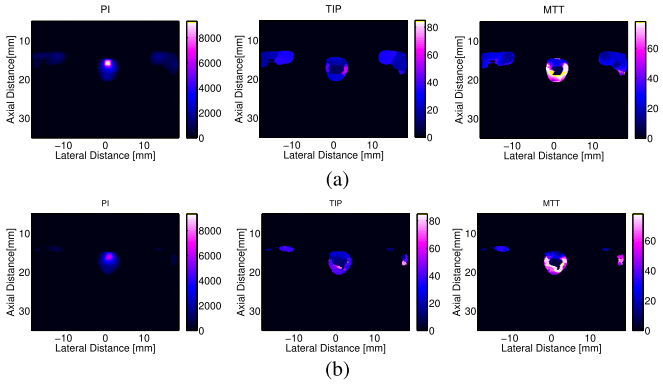

Fig. 14. Flow phantom: parametric maps for PI, TIP, and MTT (from left to right) for (a) 2-D PWI and (b) PWI central plane (3-D).

that comprised of high-frequency contrast signal [11]. Further evidence for the spread of signal due to these high-frequency grating lobes was confirmed here with flow phantom data, which demonstrated high levels of signal correlation between signal in the vessel and the regions lateral to the vessel in the background media. It should be noted that for PWI, in addition to grating lobes artifacts, the broader beam can also lead to higher correlation, because it averages signals from all points in the field of view. Furthermore, the contrast ratio calculated for 3-D center plane FI and PWI (Table I) showed a notable decrease in the average PI of the cartridge to the background for PWI compared to FI which is in agreement with the above-mentioned hypothesis.

The 3-D DCE-US central plane (3-D) correlation map showed increased correlation across the phantom for PWI compared to 2-D DCE-US correlation plane, obtained at the same position in the phantom. When acquiring the 3-D DCE-US data, the transducer is sweeping and there was also motion of the contrast agent; consequently, there was a difference in the position of the transducer when the contrast signal is collected from each of the seven angles. At 10 mm/s, largest separation in positions is small, ∼0.02 mm; however, this may reduce the coherence of the signal compounded at different angles leading to a contrast loss of signal and flattening of the TAC. This effect was previously observed [9] when we examined the shape of the TAC as a function of the number of compounding angles. A greater number of angles (7 and 11 compared to 3) reduced the PI and smoothed the TAC. In that case, only the motion of the contrast agent (with the same flow speed) was present, whereas in this case, there is the additional motion of the transducer. This smoothing of the curve may explain the small increase in correlation when the transducer is moving, as the TACs have fewer high temporal frequency components making their shape less unique, i.e., more correlated.

In addition to grating lobe artifacts, rescattering of ultrasound signal was also observed. Rescattered contrast signal is detected at a later time point and therefore appears at a greater depth in the image compared to the region from which it was scattered. The amplitude of the scattered signal is low, which was evident in both FI and PWI correlation maps, below the cartridge phantom and the vessel (Figs. 9, 11, 13, and 15). The amplitude of the rescattered signal and its correlation with signal from the cartridge phantom were greater than that of the flow phantom (correlation of ∼0.8 compared to ∼0.5, correspondingly). This was expected due to the highly scattering nature of the microvessels in the cartridge phantom. This rescattered signal will have the same effect on the spatial resolution with which spatial heterogeneity of perfusion can be mapped; however, the amplitude of the rescattered signal is very small compared to both the signal in the cartridge phantom and the vessel (Figs. 9 and 11) and compared to the signal from the grating lobes (Figs. 13 and 15). It can also be observed that there is an increase in contrast signal in the water surrounding the cartridge phantom during FI and PWI 3-D DCE-US [see TAC for point (50,50) in Figs. 9(b) and 11(b)]. This is due to a leak from the cartridge (a hole was cut in the top of the casing of the cartridge to enable acoustic access) and subsequent mixing of microbubbles in the water

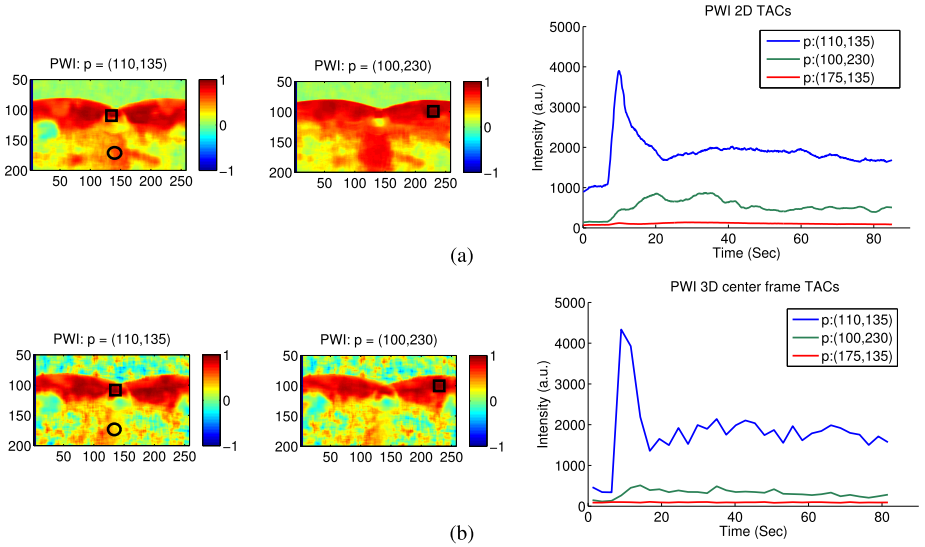

Fig. 15. Flow phantom: correlation maps for two reference points at (row, column) (from left to right): p1:(110,135) and p2:(100,230) marked as black squares in each panel and their corresponding TACs in addition to the TAC for p3:(175,135) (marked as black circle) for (a) 2-D PWI and (b) PWI for central plane (3-D).

as the transducer moves back and forth and/or the generation of bubbles from the transducer motion. This hypothesis is supported by the observation that an increase in signal is not observed in the flow phantom, for which the background is tissue-equivalent medium.

Increased correlation across the phantom supports the use of FI rather than PWI if we wish to perform 3-D parametric imaging. This blurring of signal will reduce the ability to map inhomogeneity of vascular perfusion [26]. This reduction will depend on the relative strength of the grating lobe signal or rescattered signal compared to actual contrast signal and the spatial variation in signal. If, for example, there is a low signal contrast region adjacent to a high signal region, contrast signal from grating lobes from the high signal region may have significant influence on the signal in the low contrast region. It also has implications for techniques which rely on the measurement of the spatiotemporal correlation of TACs within adjacent pixels such contrast-ultrasound dispersion imaging (CUDI). CUDI aims to map the spatial variation in vessel density and tortuosity [27]. One limitation of this study was the limited speed (up to 20 mm/s) and acceleration with which we could move the transducer. This was limited due to creation of waves within the water tank and the uneven (juddery motion) of the transducer when the magnitude of the acceleration was too great. However, we found that clinically realistic TACs could be adequately sampled using a low volume rate (0.4 Hz), and therefore if these volume rates can be used, it is expected that motion artifacts will be minimal.

V. Conclusion

The 3-D DCE-US acquired using a swept 1-D array transducer can provide accurate measurement of TAC at low volume rates (0.4 Hz). Sweep speeds of up to 20 mm/s were not observed to affect the 3-D TACs. Compared to using FI, both 2-D and 3-D DCE-USs acquired using PWI were found to be more susceptible to spatial blurring of contrast signal which was due to PWI grating lobe artifacts. There was a small increase in the correlation of contrast signal across the phantom for 3-D DCE-US acquired using PWI compared to 2-D DCE-US acquired using PWI. Spatial blurring of contrast signal may adversely affect the spatial resolution with which heterogeneity of TAC metrics of perfusion can be mapped.

Acknowledgment

The views expressed are those of the author(s) and not necessarily those of the NIHR or the Department of Health and Social Care. This research project was funded/supported by Cancer Research UK under Programme Foundation Award (C20892/A23557).

References

[1] G. Nishimura et al., "Imaging strategy for response evaluation to chemoradiotherapy of the nodal disease in patients with head and neck squamous cell carcinoma," *Int. J. Clin. Oncol.*, vol. 21, no. 4, pp. 658–667, Aug. 2016.

[2] K. Tawada et al., "Changes in tumor vascularity depicted by contrast-enhanced ultrasonography as a predictor of chemotherapeutic effect in patients with unresectable pancreatic cancer," *Pancreas*, vol. 38, no. 1, pp. 30–35, 2009.

[3] B. Pritt, T. Ashikaga, R. G. Oppenheimer, and D. L. Weaver, "Influence of breast cancer histology on the relationship between ultrasound and pathology tumor size measurements," *Mod. Pathol.*, vol. 17, no. 8, pp. 905–910, Aug. 2004.

[4] A. M. Bosch et al., "Preoperative estimation of the pathological breast tumour size by physical examination, mammography and ultrasound: A prospective study on 105 invasive tumours," *Eur. J. Radiol.*, vol. 48, no. 3, pp. 285–292, Dec. 2003.

[5] L. Hlatky, P. Hahnfeldt, and J. Folkman, "Clinical application of antiangiogenic therapy: Microvessel density, what it does and doesn't tell us," *J. Nat. Cancer Inst.*, vol. 94, no. 12, pp. 883–893, Jun. 2002.

[6] J.-W. Wang et al., "Assessment of early tumor response to cytotoxic chemotherapy with dynamic contrast-enhanced ultrasound in human breast cancer xenografts," *PLoS ONE*, vol. 8, no. 3, 2013, Art. no. e58274.

[7] G. C. Jayson, R. Kerbel, L. M. Ellis, and A. L. Harris, "Antiangiogenic therapy in oncology: Current status and future directions," *Lancet*, vol. 388, no. 10043, pp. 518–529, Jul. 2016.

[8] J. Y. Lu, J. Cheng, and J. Wang, "High frame rate imaging system for limited diffraction array beam imaging with square-wave aperture weightings high frame rate imaging system for limited diffraction array beam imaging with square-wave aperture weightings," *IEEE Trans. Ultrason., Ferroelectr., Freq. Control*, vol. 53, no. 10, pp. 1796–1812, Oct. 2006.

[9] E. Moghimirad, J. Bamber, and E. Harris, "Dynamic contrast enhanced ultrasound imaging; the effect of imaging modes and parameter settings for a microvascular phantom," in *Proc. IEEE Int. Ultrason. Symp. (IUS)*, Oct. 2018, pp. 1–8.
[10] E. Moghimirad, J. Bamber, and E. Harris, "Plane wave versus focused transmissions for contrast enhanced ultrasound imaging: The role of parameter settings and the effects of flow rate on contrast measurements," *Phys. Med. Biol.*, vol. 64, no. 9, 2019, Art. no. 095003.
[11] E. Moghimirad, J. Bamber, and E. Harris, "The impact of grating lobe clutter on plane wave DCE-US parametric imaging," in *Proc. IEEE Int. Ultrason. Symp. (IUS)*, Sep. 2020, pp. 1–4.
[12] S. M. Bentzen and V. Gregoire, "Molecular imaging–based dose painting: A novel paradigm for radiation therapy prescription," *Seminars Radiat. Oncol.*, vol. 21, no. 2, pp. 101–110, Apr. 2011.
[13] A. El Kaffas et al., "Spatial characterization of tumor perfusion properties from 3D DCE-US perfusion maps are early predictors of cancer treatment response," *Sci. Rep.*, vol. 10, no. 1, p. 11, Apr. 2020.
[14] H. Wang, O. F. Kaneko, L. Tian, D. Hristov, and J. K. Willmann, "Three-dimensional ultrasound molecular imaging of angiogenesis in colon cancer using a clinical matrix array ultrasound transducer," *Investigative Radiol.*, vol. 50, no. 5, pp. 322–329, May 2015.
[15] K. Hoyt, A. Sorace, and R. Saini, "Quantitative mapping of tumor vascularity using volumetric contrast-enhanced ultrasound," *Investigative Radiol.*, vol. 47, no. 3, pp. 167–174, Mar. 2012.
[16] K. Hoyt, A. Sorace, and R. Saini, "Volumetric contrast-enhanced ultrasound imaging to assess early response to apoptosis-inducing anti-death receptor 5 antibody therapy in a breast cancer animal model," *J. Ultrasound Med.*, vol. 31, no. 11, pp. 1759–1766, Nov. 2012.
[17] S. Feingold, R. Gessner, I. M. Guracar, and P. A. Dayton, "Quantitative volumetric perfusion mapping of the microvasculature using contrast ultrasound," *Invest Radiol.*, vol. 45, no. 10, pp. 669–674, 2010.
[18] H. Mulvana, E. Stride, M.-X. Tang, J. V. Hajnal, and R. J. Eckersley, "The influence of gas saturation on microbubble stability," *Ultrasound Med. Biol.*, vol. 38, no. 6, pp. 1097–1100, 2012.
[19] E. N. Marieb and K. Hoehn, *The Cardiovascular System: Blood Vessels Human Anatomy and Physiology*, 9th ed. Hoboken, NJ, USA: Pearson, 2013, p. 712.
[20] D. H. Simpson, C. T. Chin, and P. N. Burns, "Pulse inversion Doppler: A new method for detecting nonlinear echoes from microbubble contrast agents," *IEEE Trans. Ultrason., Ferroelectr., Freq. Control*, vol. 46, no. 2, pp. 372–382, Mar. 2002.
[21] M.-X. Tang et al., "Quantitative contrast-enhanced ultrasound imaging: A review of sources of variability," *Interface Focus*, vol. 1, no. 4, pp. 520–539, May 2011.
[22] J. Viti, H. J. Vos, N. de Jong, F. Guidi, and P. Tortoli, "Detection of contrast agents: Plane wave versus focused transmission," *IEEE Trans. Ultrason., Ferroelectr., Freq. Control*, vol. 63, no. 2, pp. 2676–2683, Feb. 2016.
[23] B. Denarie et al., "Coherent plane wave compounding for very high frame rate ultrasonography of rapidly moving targets," *IEEE Trans. Med. Imag.*, vol. 32, no. 7, pp. 1265–1276, Jul. 2013.
[24] M. Mahoney, A. Sorace, J. Warram, S. Samuel, and K. Hoyt, "Volumetric contrast-enhanced ultrasound imaging of renal perfusion," *J. Ultrasound Med.*, vol. 33, no. 8, pp. 1427–1437, Aug. 2014.
[25] S.-M. Ruan et al., "Comparison of real-time two-dimensional and three-dimensional contrast-enhanced ultrasound to quantify flow in an *in vitro* model: A feasibility study," *Med. Sci. Monitor, Int. Med. J. Exp. Clin. Res.*, vol. 25, pp. 10029–10035, Dec. 2019.
[26] J. Zhou et al., "Early prediction of tumor response to bevacizumab treatment in murine colon cancer models using three-dimensional dynamic contrast-enhanced ultrasound imaging," *Angiogenesis*, vol. 20, no. 4, pp. 547–555, 2017.
[27] M. P. J. Kuenen, T. A. Saidov, H. Wijkstra, J. M. C. H. de La Rosette, and M. Mischi, "Correspondence–spatiotemporal correlation of ultrasound contrast agent dilution curves for angiogenesis localization by dispersion imaging," *IEEE Trans. Ultrason., Ferroelectr., Freq. Control*, vol. 60, no. 12, pp. 2665–2669, Dec. 2013.

Elahe Moghimirad received the M.Sc. degree in biomedical engineering from the University of Tehran, Tehran, Iran, in 2008, and the Ph.D. degree in biomedical engineering from Tarbiat Modares University, Tehran, in 2015. She has worked on signal and image processing as a Research and Development Engineer from 2008 to 2011. During her Ph.D. degree, she formulated a novel Fourier beamformation algorithm and spent a year with the Center for Fast Ultrasound Imaging (CFU), Technical University of Denmark (DTU), Kongens Lyngby, Denmark, as a Research Visitor. She has joined the Institute of Cancer Research (ICR), London, U.K., in 2016, where she has developed a novel 3-D contrast-enhanced ultrasound imaging system to predict cancer response to therapy. Her research interests include biomedical signal and image processing, array signal processing, Fourier beamformation, and contrast-enhanced ultrasound imaging.

Zhiting Xu, photograph and biography not available at the time of publication.

Hong Ding, photograph and biography not available at the time of publication.

Jeffrey Bamber received the M.Sc. degree in developing microthermal measurement of diagnostic ultrasound power from the Chelsea College, University of London, London, U.K., in 1974, and the Ph.D. degree in the ultrasonic characterization of cancer from the Institute of Cancer Research, University of London, in 1980.

He is the Deputy Dean (Biomedical Sciences) of the Institute of Cancer Research (ICR), London. He has honorary appointments with the Royal Marsden and other hospitals. He greatly values collaborations with colleagues in the medical and biological sciences to carry out clinical and preclinical studies.

Dr. Bamber is a member of the ICR's Board of Trustees, the Institute of Physics, the British Medical Ultrasound Society, the Institute of Electrical and Electronic Engineers, the Society of Photo-Optical Instrumentation Engineers, and the International Society for Biophysics and Imaging of the Skin. He is the Vice-President of the IBUS Breast Imaging School, the past President of the International Association for Breast Ultrasound, and the past Vice-President of the International Society of Skin Imaging. He has been a Visiting Scientist at the University of Western Australia, Perth, Australia, the Tokyo Institute of Technology, Tokyo, Japan, and the Medical Products Group, Hewlett-Packard, Andover, MA, USA.

Emma Harris received the Ph.D. degree in radiation physics from University College London, London, U.K., in 2002.

She joined the Joint Department of Physics, Institute of Cancer Research (ICR) and the Royal Marsden, London, as a Postdoctoral Training Fellow to apply her expertise in physics and imaging to improve the efficacy of radiation delivery to patients with cancer. Her Ph.D. project investigated novel radiation detectors and their application to X-ray diffraction imaging for the detection of breast cancer. Since joining the ICR, her research has been focused on both X-ray and ultrasound imaging to improve the precision of radiotherapy. She continues to develop novel image guidance techniques and their clinical translation, and more recently her laboratory focuses on the development of ultrasound imaging techniques for monitoring the response of tumors to therapy.

Dr. Harris is a member of the Institute of Physics and the Institute of Electrical and Electronic Engineers. She was awarded an ICR Career Development Faculty Startup Grant in 2013 and a CRUK Program Foundation Award in 2017. She was appointed as a Reader in 2018.